SHAPE CORRECTION ALGORITHM BY COMPARING SHAPE SILHOUETTE-LINES WITH A SINOGRAM

Trung Vuong PHAM[1], Yutaka OHTAKE[1], Yukie NAGAI[1], Hiromasa SUZUKI[1]

1 School of Engineering, The University of Tokyo
Hongo 7-3-1, Bunkyo, Tokyo 113-8656, JAPAN
Email :{pham, ohtake, yukie, suzuki} @den.t.u-tokyo.ac.jp

Abstract:
In industrial X-ray CT application, there is an increasing demand for achieving accurate surface reconstruction of measured objects for dimensional inspection of mechanical parts since the performance of industrial X-ray CT scanners is considerably improved. In this paper, we propose a novel method that reuses X-ray projection images, or a sinogram, to improve the accuracy of the reconstructed surface mesh by correcting the CT values, which is done by fitting silhouette-lines of the mesh to the sinogram. The sinogram is conventionally used only for obtaining a CT volume data, or a tomogram. Since it has become capable to extract the silhouette-lines correctly regardless of beam hardening etc., reusing the sinogram has the potential application for improving the accuracy of the reconstructed mesh.

Keywords: X-ray computed tomography, shape silhouette-lines, shape correction

1. INTRODUCTION

Nowadays, industrial X-ray CT scanners have become powerful non-destructive and non-invasive tools for various applications in research, production and quality insurance. However, it is often difficult to accurately reconstruct the shape of a measured object, which is caused by CT artifacts such as metal artifacts, beam hardening, and cone-beam artifacts.

The blue arrows of Figure 1 shows the basic principle of the CT process used in this study. As a result of X-ray scanning, a series of 2D gray scale images captured from different angles, known as a *sinogram*, is obtained on the detector. On the basis of this sinogram, a CT volume data is generated by a CT reconstruction algorithm [1]. Once the CT volume data is obtained, an isosurface is typically extracted by using polygonization algorithms such as Marching Cubes [2]. When using this mesh for geometric dimensioning and tolerancing (GD&T), its geometrical accuracy is a critical parameter. However, in some cases, the isosurface mesh reconstruction of objects is not sufficiently accurate because the CT volume data is not accurately generated. The sinogram is conventionally used only for reconstructing the CT volume data. We propose a novel method for improving the accuracy of the polygonal mesh by reusing the sinogram as shown in the red arrows of Figure 1.

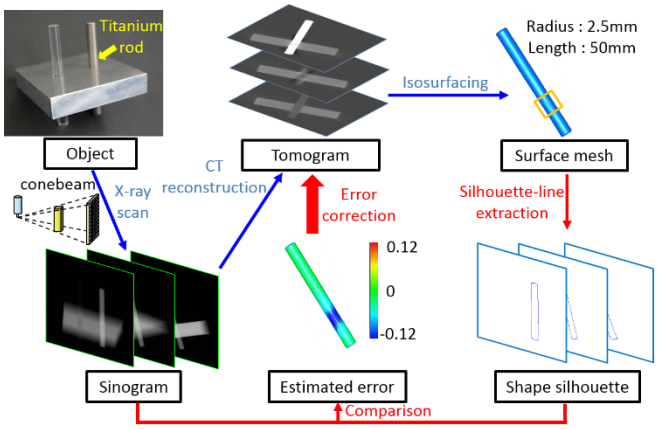

Figure 1. Algorithm overview. The blue arrows show the conventional CT process and the red arrows indicate our proposed shape correction method.

The essence of this method is that it is possible to detect the silhouette-lines precisely regardless of CT artifacts. The fundamental concept of the proposed method is to estimate errors of mesh vertices in the normal directions by comparing silhouette-lines of the surface mesh with the sinogram. On the basis of the estimated errors, we modify the CT values of the initial CT volumetric data. Additionally, we aim to achieve sub-pixel accuracy of detector size by interpolating the sinogram when computing fitting errors of the silhouette-lines.

2. METHOD

2.1 Shape silhouette-lines extraction

The shape silhouette-lines on a continuous surface are the sets of points whose normal vectors are perpendicular to the view direction (Figure 2(a)). In other word, the silhouette-lines comprise the set of points that satisfy

$$d(\boldsymbol{p}) \equiv \boldsymbol{n}(\boldsymbol{p}) \cdot (\boldsymbol{p} - \boldsymbol{c}) = 0, \quad (1)$$

where $\boldsymbol{p}$ is a point on the surface, $\boldsymbol{n}(\boldsymbol{p})$is the unit normal vector at $\boldsymbol{p}$, and $\boldsymbol{c}$ is a perspective viewpoint [3]. Considering the focal point of the X-ray source as the viewpoint, the procedure of obtaining the silhouette is as follows:

1. For each mesh triangle consisting of vertices $\boldsymbol{p}_A$, $\boldsymbol{p}_B$, and $\boldsymbol{p}_C$, the dot products $d(\boldsymbol{p}_A)$, $d(\boldsymbol{p}_B)$, and $d(\boldsymbol{p}_C)$ are computed, respectively. Then the silhouette points are located where $d(\boldsymbol{p}) = 0$ by linearly interpolating the values of d on the triangle. For example, silhouette points $\boldsymbol{a}$ and $\boldsymbol{b}$ in Figure 2(b) are located as such that

$$\boldsymbol{a} = \frac{|d(\boldsymbol{p}_A)|\boldsymbol{p}_B + |d(\boldsymbol{p}_B)|\boldsymbol{p}_A}{|d(\boldsymbol{p}_A)| + |d(\boldsymbol{p}_B)|},$$
$$\boldsymbol{b} = \frac{|d(\boldsymbol{p}_A)|\boldsymbol{p}_C + |d(\boldsymbol{p}_C)|\boldsymbol{p}_A}{|d(\boldsymbol{p}_A)| + |d(\boldsymbol{p}_C)|}. \quad (2)$$

   Next, line segments are created by connecting the points to form the silhouette-lines (Figure 2(c)). Normal vectors of silhouette points are also computed for the next step.
2. In order to obtain the 2D silhouette-lines and their normal vectors on the detector plane, perspective projection is

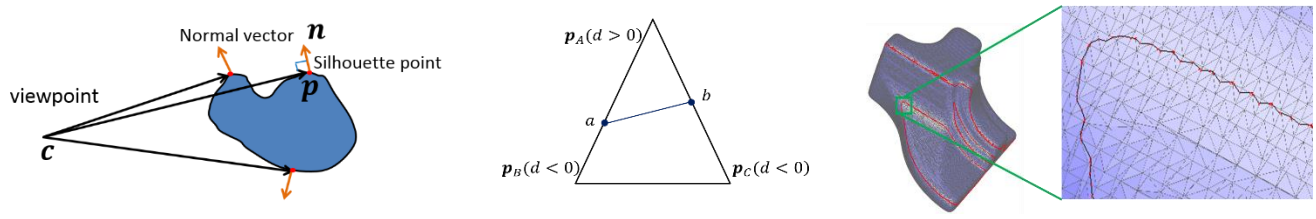

(a) (b) (c)

Figure 2. Silhouette-lines extraction. (a) The concept of silhouette-lines extraction. (b) Silhouette points computed by linear interpolation. (c) Silhouette-lines created by connecting the line segments.

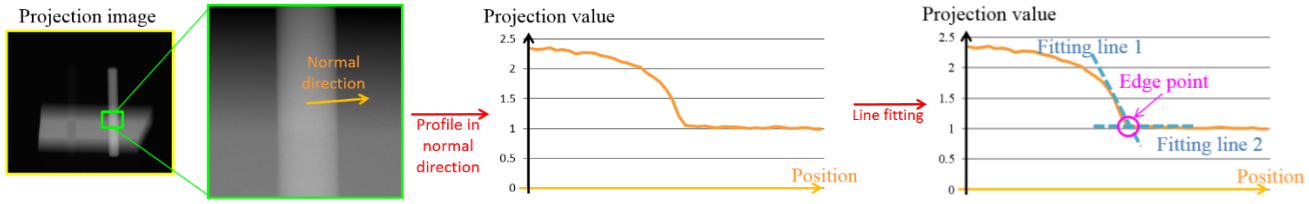

(a) (b)

Figure 3. The concept of the edge search. (a) Gray value along the normal direction. (c) Approach of edge point search.

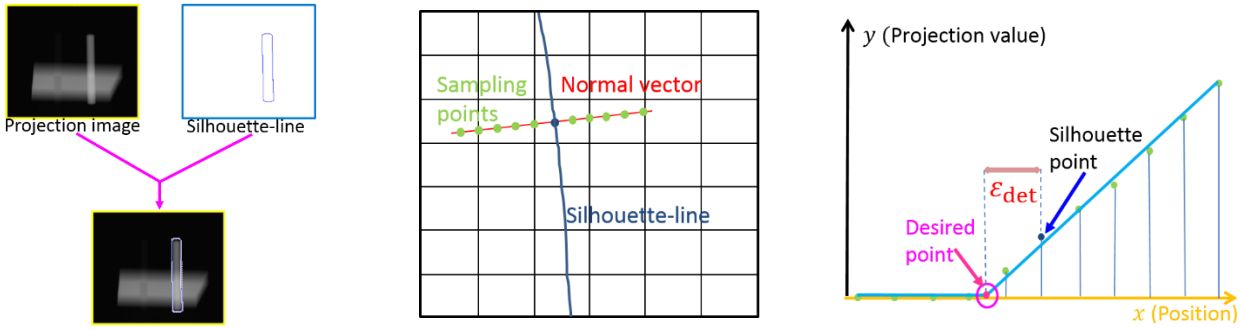

(a) (b) (c)

Figure 4. (a) Silhouette-lines and projection image in the same coordinate. (b) Sampling points close to a silhouette point in the normal vector direction. (c) Computation of the fitting error.

performed for the 3D silhouette-lines and their normal vectors determined in Step 1.

2.2 Fitting-error computation

We estimate the planar errors by comparing the silhouette-lines on the detector with the projection image which has a same projection image. According to the aforementioned definition, the silhouette-lines correspond to the edges of the projection image; therefore, the fitting errors are the differences between the edges and the silhouette-lines. Moreover, because of the inherent property of the projection image, the gradient of the projection value at every edge point changes abruptly (Figure 3(a)). On the basis of this property, the edge point is considered as an intersection of two fitting lines of sampling points adjacent in the normal direction of each silhouette point (Figure 3(b)).

The procedure for fitting-error computation is as follows:

1. First, we put the silhouette-lines on the detector and the projection image having the same projection angle in the same coordinate (Figure 4(a)).
2. Then, q times of pixel pitch close to each silhouette point in the normal vector direction are selected, and h sampling points for each pixel pitch are generated (Figure 4(b)). Projection values of sampling points are computed by bilinear interpolation. Assuming that the number of sampling points is $n = qh$, we divide the sampling points into two subsets: $[1, k]$ and $[k+1, n]$, where $k \epsilon [3, n-3]$ is index of point of interest. For each group, we fit a straight line to the data by using the least square method [4]. Assuming that the fitting lines are $y_1 = a_1 x + b_1$ and $y_2 = a_2 x + b_2$, we then find the best dividing position k_{opt}, at which the sum of residuals $S(k)$ is minimal (Figure 4(c)):

$$k_{\text{opt}} = \arg\min_k S(k),$$
$$S^2(k) = \sum_{i=1}^{k} (y_1 - (a_1 x_i + b_1))^2 + \sum_{j=k+1}^{n} (y_2 - (a_2 x_j + b_2))^2. \quad (3)$$

3. Next, we find the intersection of two fitting lines and consider the difference between the intersection and the corresponding silhouette point as the fitting error ε_{det} as follows, where δ is the pixel size of the projection image:

$$\varepsilon_{det} = \frac{\delta}{h}\left(\frac{b_2 - b_1}{a_2 - a_1} - \frac{q}{2}\right). \quad (4)$$

2.3 Computation of the polygonal silhouette-lines error

In this section, we apply back-projection of the fitting errors to the polygonal mesh to obtain the positional error at each silhouette point. For each projection image, the back-projection error of each silhouette point ε can be computed as

follows, where ε_{det} is the fitting error on the detector, L is the distance between the X-ray source and the object, D is the distance between the X-ray source and the detector, λ is the angle between the focal axis and the view vector, $\|\boldsymbol{c}-\boldsymbol{p}\|$ is the distance between the X-ray source and the silhouette point (Figure 5):

$$\varepsilon = \varepsilon_{\text{det}} \frac{L}{D} \cos\lambda = \varepsilon_{\text{det}} \frac{L^2}{D\|\boldsymbol{c}-\boldsymbol{p}\|}. \quad (5)$$

The polygonal mesh is sequentially rotated and compared with the equivalent projection image to compute the corresponding errors of the mesh vertices. We repeat the abovementioned steps until all projection images have been compared. The overall estimated error of each silhouette point $E(\boldsymbol{p})$ is a mean value of its total error and its number of repetition $M(\boldsymbol{p})$ during the error-mapping process:

$$E(\boldsymbol{p}) = \frac{1}{M(\boldsymbol{p})} \sum_{t=1}^{M(\boldsymbol{p})} \varepsilon_t(\boldsymbol{p}), \quad (6)$$

where $\varepsilon_t(\boldsymbol{p})$ is the t-th back-projection error at silhouette point $\boldsymbol{p}$.

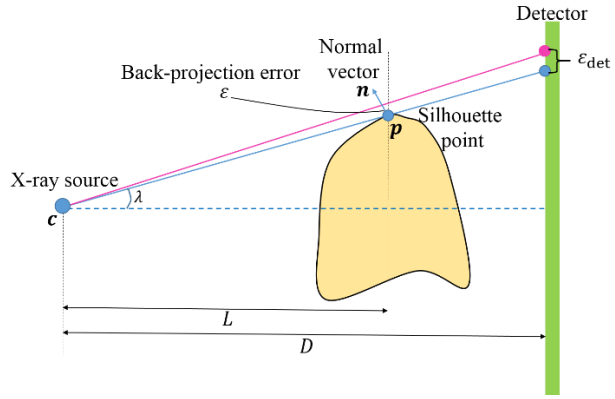

Figure 5. Back-projection of the error.

2.4 CT volume correction

We then correct the CT values of the CT volume based on the estimated errors. Thus the equivalent polygonal mesh extracted from the corrected CT volume with the same isovalue will become more accurate than the initial surface mesh (Figure 6). First, on the basis of the estimated error at each silhouette point, we compute the corresponding error at each voxel of the CT volume using the weighted coefficients based on the normal distribution $\exp(-d^2/2r^2)$, where r is a searching range, d is the distance between the focusing silhouette point and a voxel lying inside the searching range (Figure 7). After completing the error-mapping process, the appropriate error $\sigma(V)$ of each voxel V is the mean value of its mapping-errors and its coefficients as follows:

$$\sigma(V) = \frac{\sum_{t=1}^{k} E_t \exp(-d_t^2/2r^2)}{\sum_{t=1}^{k} \exp(-d_t^2/2r^2)}. \quad (7)$$

Then we modify the CT value of each voxel using gradient flow that controls surface deformation in the normal direction [5] as follows:

$$v \leftarrow v + \sigma(V)\|\nabla v\|, \quad (8)$$

where v is the CT value and $\|\nabla v\|$ is magnitude of the gradient at the voxel V. In order to obtain more precise result, the gradient ∇v is estimated by upwind scheme [6]. The target surface will deform outward or inward offset depending on the sign of the error $\sigma(V)$.

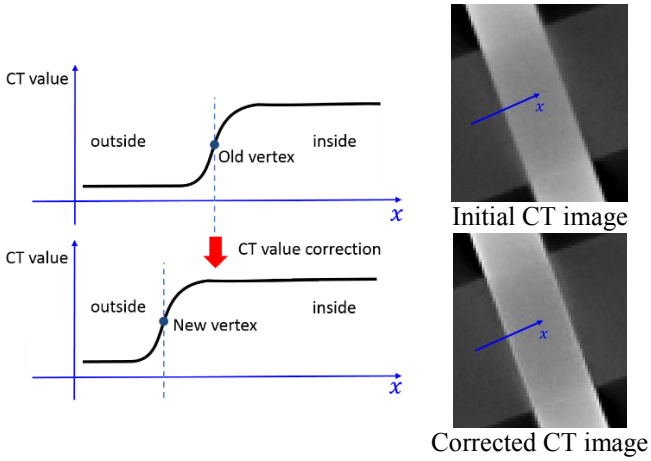

Figure 6. Concept of CT value correction

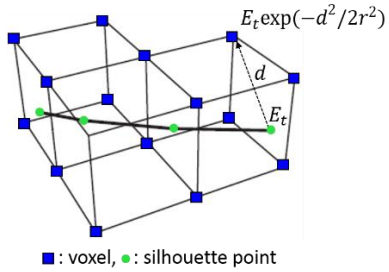

Figure 7. Error-mapping from silhouette points to voxels.

2.5 Summary of the Method

The proposed algorithm can be summarized as follows:

1. Extract the silhouette-lines of the surface mesh considering the focal point of the X-ray source as a viewpoint. Then perform the perspective projection of the silhouette-lines on the detector.
2. Compute the fitting errors by comparing the silhouette-lines on the detector with the sinogram.
3. Apply back-projection of the fitting errors to the polygonal mesh to obtain the estimated errors at each silhouette points.
4. Correct the CT values of the CT volume based on the estimated errors. Then extract the equivalent polygonal mesh which has the same isovalue with the initial surface mesh.

3. RESULTS AND DISCUSSION

3.1 Experiment conditions

The proposed method was applied to both simulation data and actual scanned data. The simulation data was obtained by using Scorpius Xlab software for cone-beam X-ray CT scanner simulation. The actual scanned data was obtained by using Carl Zeiss Metrotom 800 cone-beam X-ray CT scanner. Isosurface meshes were obtained by using the Marching Cubes technique [2] from the volume data. The experiment

Table 1. Experiment conditions

Experiment data	Sphere (Iron) 	Rod (Titanium) 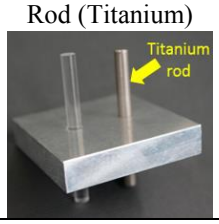	Pedal part (Aluminum) 	Plate (Iron) 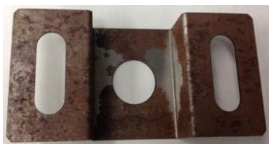
Voltage (kV)	120	100	120	125
Current (mA)	0.5	0.15	0.15	0.15
Number of pixel	500×500	728×920	728×920	728×920
Pixel size (mm)	0.03	0.12	0.16	0.14
Projection numbers	500	800	800	800

conditions are shown in Table 1. The sinogram of the Sphere is the simulation data and the remains are actual scanned data. Moreover, the number of adjacent pixels of each silhouette point is $q = 4$, the sampling rate of each pixel is $h = 4$, and the searching range of CT volume correction is $r = 3$ voxels in the vicinity in all cases.

3.2 Results

Figure 8 shows the result of the iron sphere with a 5.0 mm radius. Due to the cone-beam artifact, the reconstructed CT volume contains partial volume artifacts locating in the vicinity of the poles (Figure 8(b)). We evaluate the error by comparing both initial and corrected shape with the perfect sphere (Figure 8(c)). Shape improvement is clearly visible. The radius of the corrected sphere was 4.99 mm, whereas that of the initial sphere was 4.97 mm. Moreover, sphericity of the corrected and initial spheres are 0.06 and 0.10, respectively. Note that mesh vertices locating in the vicinity of the poles were not used in computing the radii and the sphericity.

Figure 9 shows the result of actual scanned data for a titanium rod with a 2.5 mm radius. Due to the beam hardening artifact of the CT image (Figure 9(b)), the initial shape shows a conspicuous dent, which is not present in the corrected shape (Figure 9(c)). We evaluate the error by actually measuring the defect parts both initial and corrected shape with the CAD model of the rod. As a consequence, the radius of the defect part is 2.39 mm in the initial shape, and 2.49 mm in the corrected shape. Therefore, improvement of the dimension of the data is remarkably apparent.

Figure 10 shows the result of actual scanned data for an Aluminum pedal part. We tried to evaluate the diameters of cylinder marked with pink arrows shown in Figure 10(a). Due to the beam hardening, these parts of the reconstructed shape should become slightly smaller than the actual ones. The result of actual measurement is $D_1 = D_2 = 13.95$ mm. The result of initial shape is $D_1 = 13.78$ mm and $D_2 = 13.71$ mm. The result of corrected shape is 13.87 mm and 13.89 mm respectively. In Figure 10(d), the dark grey indicates the areas that are not be able to be evaluated by the proposed method. These areas were put almost parallel with the X-ray projected direction, so the proposed method could not detect the silhouette-lines properly.

Figure 11 shows the result of a thin iron plate with thickness of 1.0 mm. Due to the metal artifact of the CT image (Figure 11(b)), the initial reconstructed shape show critical defects. We tried to evaluate the alteration of thickness of the plate by measuring the part marked with purple arrows shown in Figure 11(c) and (e). As a consequence, the thickness of the initial shape and the corrected shape is 1.27 mm and 1.14 mm, respectively. This improvement is appropriate with the error evaluation of the initial shape shown in Figure 11(d). However, no improvement can be expected with the part marked with red circles. It means that our method could be not suitable with parts that have significant reconstructed defects.

In summary, Table 2 shows the results of quantitative evaluation of the proposed method.

Table 2. Results of quantitative evaluation (proposed method)

(Unit: mm)		Ideal	Initial	Our method
Sphere	r	5.00	4.97	4.99
Rod	R	2.50	2.39	2.49
Pedal	D_1	13.95	13.78	13.87
	D_2	13.95	13.71	13.89
Plate	t	1.00	1.27	1.14

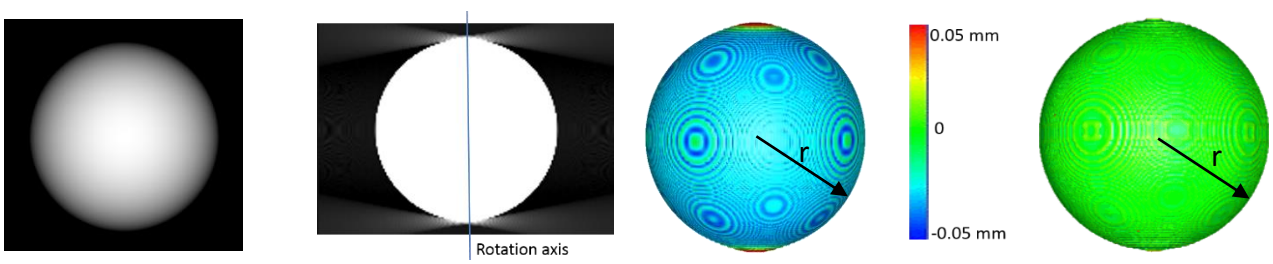

(a) (b) (c)

Figure 8. Results of sphere experiment (radius = 5 mm). (a) Sinogram. (b) Cross-section of CT volume. (c) Error color-map of initial and corrected shape.

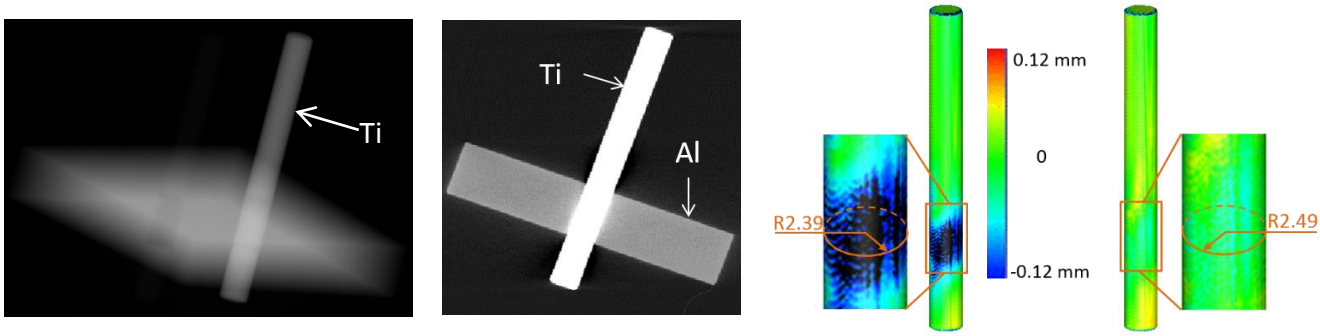

(a) (b) (c)

Figure 9. Results of rod experiment (radius = 2.5 mm). (a) Sinogram. (b) Cross-section of CT volume. (c) Comparison of initial and corrected shape.

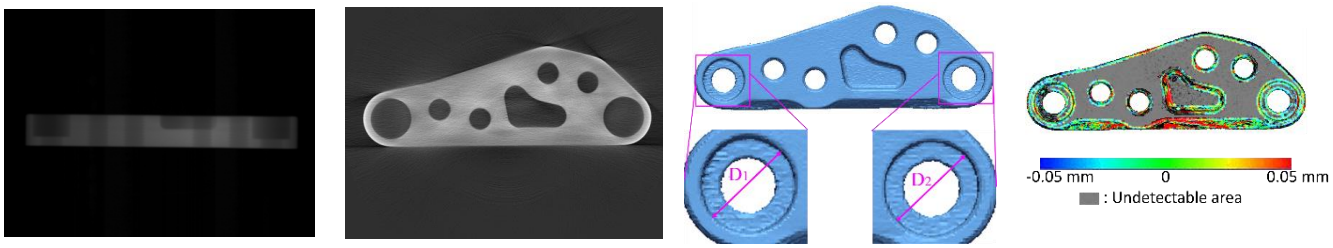

(a) (b) (c) (d)

Figure 10. Results of pedal experiment (radius = 5 mm). (a) Sinogram. (b) Cross-section of CT volume. (c). Initial shape. (d) Error evaluation of initial shape using proposed method.

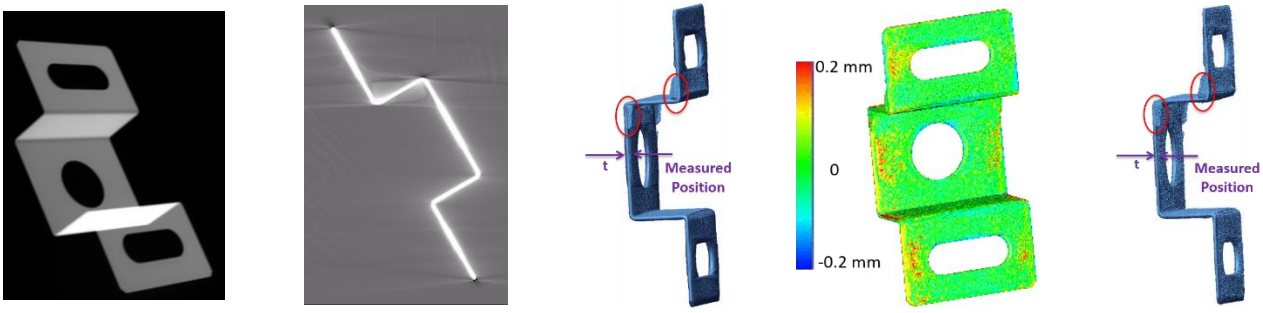

(a) (b) (c) (d) (e)

Figure 11. Results of plate (thickness = 1.0 mm). (a) Sinogram. (b) Cross-section of CT volume. (c)Initial shape. (d) Error color-map. (e) Corrected shape.

3.3 Comparison with local surface extraction method

To confirm the application of the proposed method, comparison with the local surface extraction method [7] was performed. We try to compare with this method because it has the same essence with our method that try to optimize the best position of surface mesh vertices in the corresponding normal directions.

We will give a brief description of this method. First, the anisotropic diffusion [8] is applied to the CT volume to reduce noise. Then, on the basis of the refined volume data, positions of the mesh vertices are optimized by moving the surface vertices in the direction of the corresponding point normal to a position with maximum gradient magnitude (Figure 12). As recommended in [7], the searching range is 2 voxels around each vertex in the normal direction, and 100 sampling points for each voxel are generated. The CT values of sampling points are computed by trilinear interpolation.

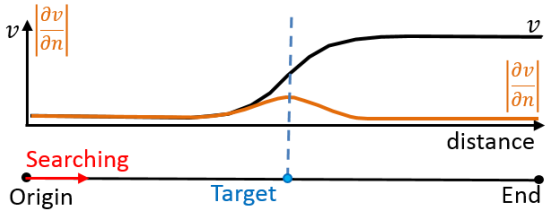

Figure 12. Search of a position of the maximum gradient magnitude.

Table 3 shows the results of the abovementioned objects corrected by the local surface extraction method. Figure 13 shows the results of error evaluation of the sphere and the rod using this method. In all cases, the proposed method gives more accurate results than the local surface method.

Accordingly, the proposed method can be considered more suitable in terms of dimensional improvement of shapes.

Table 3. Results of quantitative evaluation

(Unit: mm)		Ideal	Our method	Method [7]
Sphere	r	5.00	4.99	4.97
Rod	R	2.50	2.49	2.466
Pedal	D_1	13.95	13.87	13.86
	D_2	13.95	13.89	13.86
Plate	t	1.00	1.143	1.26

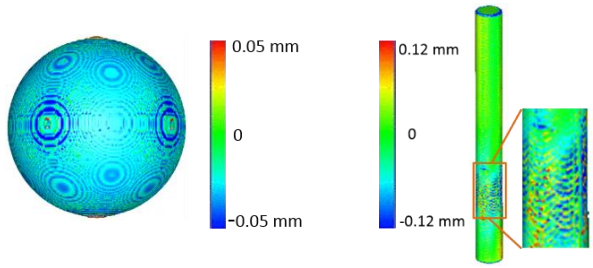

(a) (b)

Figure 13. Error evaluation using the local surface extraction method [7]. (a) Result of the sphere. (b) Result of the rod.

3.4 Limitation

The proposed method has two limitations as follows:

1. It is not applicable to parts in which the silhouette lines cannot be accurately detected. In other words, shapes that are put almost parallel with the X-ray projected direction while being scanned are not be able to be improved with proposed method.
2. Parts in which the initial reconstructed shapes show significant defects also cannot be accurately corrected. In order to resolve this problem, we consider that the sinogram needs to be preprocessed to get more accurate isosurface mesh.

4. CONCLUSION

This paper proposed a novel method for correcting the shape inaccuracy caused by CT artifacts by comparing shape silhouette lines and X-ray projection images. We demonstrated that the shape accuracies of objects having curves and pin angles, such as spheres and cylinders, are improved by applying the proposed method. In the future work, we plan to improve the method so that it can be applied to a wide range of shapes.

REFERENCES

[1] J. Hsieh, "Computed Tomography: Principles, Design, Artifacts, and Recent Advances", *SPIE PRESS*, 2003.

[2] W. E. Lorensen and H. E. Cline, "Marching cubes: A high resolution 3D surface construction algorithm", *ACM SIGGRAPH Computer Graphics*, vol. 21, pp. 163-169, 1987.

[3] D. DeCarlo, A. Finkelstein, S. Rusinkiewicz, and A. Santella, "Suggestive contours for conveying shape", *ACM Transactions on Graphics*, vol. 22, pp. 848-855, 2003.

[4] S. A. Teukolsky et al, "Numerical Recipes in C++", *Cambridge University Press*, pp.666-670, 2002.

[5] P. Mullen, et al, "A variational Approach to Eulerian Geometry Processing", *ACM Transactions on Graphics*, vol. 26, pp. 66-1 - 66-6, 2007.

[6] S. Osher, R. Fedkiw, "Level Set Methods and Dynamic Implicit Surfaces", *Springer*, pp. 57-58, 2003.

[7] C. Heinzl, J. Katsner, et al, "Surface Extraction from Multi-Material Components for Metrology using Dual Energy CT", *IEEE Trans Vis Compute Graph*, vol. 13, pp. 1520-1527, 2007.

[8] P. Perona, J. Malik, "Scale-space and edge detection using anisotropic diffusion", *IEEE Transactions on Pattern Analysis and Machine Intelligence*, vol. 12, pp. 629-639, 1990.